International Journal of Heat and Mass Transfer 64 (2013) 636–646

Contents lists available at SciVerse ScienceDirect

International Journal of Heat and Mass Transfer

journal homepage: www.elsevier.com/locate/ijhmt

An investigation of flow reversal of mixed convection in a three dimensional rectangular channel with a finite length

Wu-Shung Fu *, Yu-Chih Lai, Yun Huang, Kuan-Lan Liu

Department of Mechanical Engineering, National Chiao Tung University, Hsinchu 30010, Taiwan, ROC

ARTICLE INFO

Article history:
Received 20 August 2012
Received in revised form 15 April 2013
Accepted 15 April 2013
Available online 29 May 2013

Keywords:
Reversal flow
Mixed convection
Three dimensional channel

ABSTRACT

An investigation of flow reversal of mixed flow in a three dimensional channel is studied numerically. At a high Richardson number, natural convection dominates the flow and thermal fields of mixed convection. Behaviors of the residual mass flow rate produced by the difference of the strength of natural and forced convections coexisting in mixed convection are worthy to be examined deeply for industrial applications. Due to the necessity of considering the fluid compressibility, methods of the Roe scheme, preconditioning and dual time stepping are adopted to solve governing equations. The results show that at a high Richardson number situation, via the outlet in large quantities of fluids are sucked into the channel from the outside that causes the flow and thermal fields in the channel to be unsteady and vice versa.

1. Introduction

Strictly speaking, except in situations of low temperature differences between cooling fluids and heat sources, heat transfer phenomena of forced convection only in realistic situations are hardly observed; instead, the coexistence of forced and natural convections, also called mixed convection, usually appears. Heat transfer phenomena of mixed convection are strongly influenced by the ratio of natural convection to forced convection. And mixed convection is mainly divided into three parts of cross, opposite and aiding flows. Due to the same direction of the buoyancy force and a fluid flow in aiding flow mixed convection, the number of analyses of aiding flow mixed convection are relatively more than those of the other two mixing flows. From a viewpoint of enhancement of heat transfer, aiding flow mixed convection is usually regarded to be advantageous, so it attracts more investigations than those of the other two types.

Metais et al. [1] conducted an experimental work to draw a diagram indicating a flow relationship between Reynolds and Grashof numbers. In the diagram, regions of natural, forced and mixed convections divided into a laminar and a turbulent flows were clearly delimited. Behzadmehr et al. [2] investigated aiding flow mixed convection with the Boussinesq assumption under conditions of uniform heat flux and low Reynolds numbers in a vertical circular duct. Relationships of Grashof and Nusselt numbers were yielded to distinguish the laminar and turbulent regions. The results showed that the regions of Re = 1000, $8 \times 10^5 < Gr < 5 \times 10^7$ and Re = 1500, $2 \times 10^6 < Gr < 10^8$ were included in the turbulent region. Tanaka et al. [3] conducted an experimental work like [1] to draw a diagram of Reynolds via Grashof numbers, the domain of Reynolds number was between 1000 and 5000. Regions of natural, forced and mixed convections were divided into the laminar and turbulent flows. Celata et al. [4] showed the experimental results of the distribution of the buoyancy parameter of Bo in a figure of Reynolds number via Grashof number with water. In the range of $Bo \leqslant 1$, a laminar phenomenon was observed, and the corresponding Nusselt number was slightly smaller than that of pure forced convection. Boulama and Galanis [5] studied aiding flow mixed convection in a two-dimensional vertical parallel plates with a condition of fully developed flow at the outlet, and the analytical solutions were dependent on the parameters which combined the effects of thermal and solutal buoyancy. The results revealed that buoyancy effects significantly improved heat and momentum transfer rates near the heated walls. Desrayaud and Lauriat [6] investigated aiding flow mixed convection of a two-dimensional vertical duct with a high wall temperature. The results showed that when the magnitude of Gr/Re^2 was larger than 1, phenomena of flow reversal were observed. Under a condition of a constant Grashof number, the larger the Reynolds number was, the more difficult the flow reversal was found. Zghal et al. [7] investigated aiding flow mixed convection in a two-dimensional vertical duct with the Boussinesq assumption. Effects of parameters of length, Reynolds number and Richardson number on Nusselt number were examined. Appearance of flow reversal was mainly determined between a relationship of Peclet and Richardson numbers. Ingham et al. [8] investigated phenomena of flow reversal of mixed

* Corresponding author. Address: 1001 Ta Hsueh Road, Hsinchu 30056, Taiwan, ROC. Tel.: +886 3 5712121x55110; fax: +886 3 5735065.
E-mail address: wsfu@mail.nctu.edu.tw (W.-S. Fu).

0017-9310/$ - see front matter © 2013 Elsevier Ltd. All rights reserved.
http://dx.doi.org/10.1016/j.ijheatmasstransfer.2013.04.025

Nomenclature

a	sound speed (m s^{-1})
A	area (m^2)
C_p	constant-pressure specific heat (J kg^{-1} k^{-1})
C_v	constant-volume specific heat (J kg^{-1} k^{-1})
d	width of the square channel (m)
e	internal energy (J kg^{-1})
g	acceleration of gravity (m s^{-2})
Gr	Grashof number defined in Eq. (12)
h	enthalpy (J)
k	thermal diffusivity (W m^{-1} k^{-1})
k_0	surrounding thermal diffusivity (W m^{-1} k^{-1})
l	length of the square channel (m)
$\dot{M}_{inlet,n.c.}$	dimensionless mass flow rate of natural convection defined in Eq. (36)
$\dot{M}_{inlet}$	dimensionless mass flow rate at inlet defined in Eq. (33) (kg s^{-1})
$\dot{M}_{outlet}$	dimensionless mass flow rate from outside at the outlet defined in Eq. (34) (kg s^{-1})
$\overline{Nu}$	area averaged Nusselt number defined in Eq. (38)
Nu_x	local Nusselt number defined in Eq. (35)
$(Nu_x)_t$	time averaged local Nusselt number defined in Eq. (37)
$(\overline{Nu})_t$	time and area averaged Nussel number defined in Eq. (39)
P	pressure (Pa)
P_0	surrounding pressure (Pa)
Pr	Prandtl number
R	gas constant (J kg^{-1} k^{-1})
Ra	Rayleigh number defined in Eq. (12)
Re	Reynolds number defined in Eq. (10)
Ri	Richardson number defined in Eq. (11)
t	time (s)
t^*	dimensionless time defined in Eq. (9)
T	temperature(K)
T^*	dimensionless temperature defined in Eq. (9)
T_0	temperature of surroundings (K)
T_h	temperature of heat surface (K)
ΔT	time difference (K)
u, v, w	velocities in x, y and z directions (m/s)
U, V, W	dimensionless velocities in x, y and z directions defined in Eq. (9)
x, y, z	Cartesian coordinates (m)
X, Y, Z	dimensionless Cartesian coordinates in Eq. (9)

Greek symbols

α	Thermal diffusivity rate (m^2/s)
β	volumetric thermal expansion coefficient (K^{-1})
ρ	density (kg m^{-3})
ρ_0	surrounding density (kg m^{-3})
υ	kinematics viscosity (m^2 s^{-1})
μ	absolute viscosity (N s/m^2)
μ_0	viscosity of surrounding (N s/m^2)
γ	specific heat ratio
Γ	preconditioning matrix [17]
δ_x, δ_y, δ_z	central-difference operators defined in Eq. (17)

convection in a two-dimensional constant temperature vertical duct with the Boussinesq assumption. In a range of $-300 \leqslant Gr/Re \leqslant 70$, the flow reversal easily appeared at the larger magnitude of $|Gr/Re|$. Barletta [9,10] adopted an analytical method and the Boussinesq assumption to investigate mixed convection in a rectangular cross-section duct with a fully developed flow condition in the z axis. Thermal conditions of walls were composed of different combinations of high and low temperatures and constant heat flux. Phenomena of flow reversal were examined under different shapes of rectangular cross section. Barletta [11] investigated viscous dissipation effect of mixed convection in a two-dimensional vertical duct. The phenomenon of flow reversal in opposing flow mixed convection was more apparent than that in aiding flow mixed convection under the Boussinesq assumption. Yang et al. [12] adopted the Boussinesq assumption to study mixed convection in a long two-dimensional vertical duct. Heat transfer mechanisms were investigated under positive and negative magnitudes of Richardson numbers. Nguyen et al. [13] investigated transient mixed convection in a high heat flux circular duct with the Boussinesq assumption numerically. Boundary conditions at the inlet and outlet were a uniform velocity and a fully developed flow, respectively. In an opposite situation, the flow reversal appeared near the outlet region at $Gr = 3 \times 10^5$, and in an aiding situation the flow reversal appeared near the center of the axis at $Gr = 10^6$.

In retrospect, the Boussinesq assumption which is only useful for the temperature differences smaller than 30 K [14] is still conveniently used by most of the above literature. According to the limitation of the Boussinesq assumption, the analysis of mixed convection is then necessary to add an extra domain to the original domain that causes a fully developed condition to be adopted at the edge of the domain newly added. Regretfully, by using the Boussinesq assumption, some interesting and important characteristics of mixed convection have the possibility to be omitted especially in the range of the high magnitude of Richardson number. Doubtless, at a high Richardson number situation natural convection dominates flow and heat transfer mechanisms. Then the amount of fluid which is induced by natural convection and flows through the domain is substantially larger than the amount of fluid which is provided by forced convection and flows through the domain. Behaviors of the residue of the fluid caused by the difference between the amount of fluid provided by forced convection and the amount of fluid induced by natural convection are not deeply discussed yet. As well, the inlet is usually filled with the amount of fluid provided by forced convection. As a result, a problem of consideration of behaviors of the residue of the fluid mentioned above becomes important and is worthy of deep investigation.

The aim of the study investigates flow reversal and heat transfer mechanisms of mixed convection in a three-dimensional vertical channel with a finite length under larger Richardson numbers numerically. A non-reflecting boundary condition is assigned at the outlet of the domain to adjust fluids sucked into the channel or discharged to the outside of the channel according to the magnitude of the Richardson number. The compressibility of fluid has been taken into consideration for matching the usage of the non-reflecting boundary condition which also means that the Boussinesq assumption is no longer needed. Necessary methods of the Roe scheme [16], preconditioning and dual time stepping [17] for solving a low speed compressible flow are used. The results show that in high Richardson number situations natural convection is dominant and causes part of the amount of fluid from the outside via the outlet to be sucked into the channel. In a certain situation, the amount of fluid sucked into the channel is approximately equal to that flowing into the channel via the inlet provided by forced convection. That leads to drastic impingement between both the

amounts of fluid mentioned above to occur and the flow field to be unsteady. Oppositely, in low Richardson number situations the amount of fluid provided by forced convection is larger than the amount of fluid sucked into the channel induced by natural convection. As a result, the impingement mentioned above becomes peaceful and the flow in the channel displays a steady situation.

2. Physical model

A physical model investigated in this study is a three-dimensional vertical rectangular channel and shown in Fig. 1. The cross section of the channel is square and the width is d. The length of the channel is finite and equal to l. The direction of gravity g is downward and parallel to the vertical channel. The temperature of four heat wall surfaces is constant and equal to T_h which is higher than a temperature T_0 of surroundings. Boundary conditions of the temperature and velocity and pressure at the outlet of the channel EFGH are non-reflecting which was developed by Fu et al. [15].

In the situation of natural convection, via the inlet the amount of fluid flowing into the channel has difficulty to be predicted in advance. Then the non-reflecting boundary conditions of the velocity, temperature and pressure are held at the inlet to determine the amount of fluid induced by natural convection and flowing into the channel and shown in Fig. 1(a).

The same channel is also used in mixed convection, the amount of fluid via the inlet flowing into the channel is provided by forced convection and evenly distributed on the inlet and shown in Fig. 1(b). The velocity and temperature of the flowing fluid are equal to u_0 and T_0, respectively. In this situation of mixed convection, the amount of fluid induced by natural convection via the inlet flows into the channel is no longer permitted because of the complete occupancy of the amount of fluid provided by forced convection at the inlet. Therefore, in a large Richardson number situation the amount of fluid induced by natural convection is permitted only from the central region of the outlet to flow downwards into the channel and compulsively impinges the amount of fluid which is provided by forced convection and flowing upwards into the channel from the inlet. Both the amounts of fluid then mix together and newly compose upward streams along the heat walls via the outlet to flow out of the channel. Phenomena of flow reversal are then to be observed in the channel.

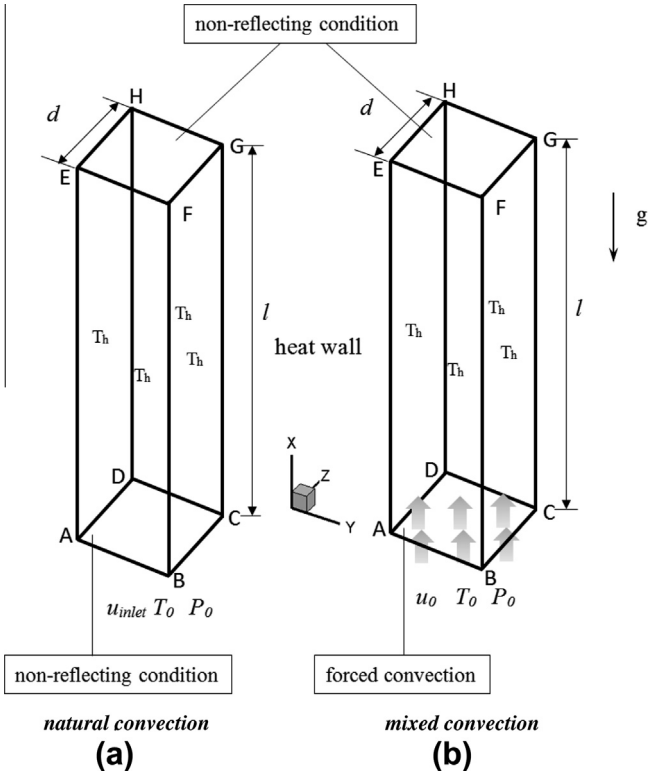

Fig. 1. Physical model.

For facilitating the analysis, several assumptions are made and indicated as follows.

(1) A laminar flow.
(2) Properties of fluids follow the equation of state of an ideal gas.
(3) The pressure gradient in normal direction of surfaces is equal to zero.

The governing equation is expressed as follows

$$\frac{\partial U}{\partial t}+\frac{\partial F_1}{\partial x}+\frac{\partial F_2}{\partial y}+\frac{\partial F_3}{\partial z}=S \tag{1}$$

The quantities included in U, F_i and S are separately shown in the following equations, respectively

$$U=\begin{pmatrix}\rho\\ \rho u\\ \rho v\\ \rho w\\ \rho e\end{pmatrix} \tag{2}$$

$$F_i=\begin{pmatrix}\rho u_i\\ \rho u_i u_1+P\delta_{i1}-\mu A_{i1}\\ \rho u_i u_2+P\delta_{i2}-\mu A_{i2}\\ \rho u_i u_3+P\delta_{i3}-\mu A_{i3}\\ (\rho e+P)u_i-\mu A_{ij}u_j-k\frac{\partial T}{\partial x_i}\end{pmatrix},\quad \forall i=1(x),2(y),3(z) \tag{3}$$

$$S=\begin{pmatrix}0\\ -(\rho-\rho_0)g\\ 0\\ 0\\ -(\rho-\rho_0)gu_1\end{pmatrix} \tag{4}$$

where $A_{ij}=\frac{\partial u_j}{\partial x_i}+\frac{\partial u_i}{\partial x_j}$ and the ideal gas equation is written by

$$P=\rho RT \tag{5}$$

On the surfaces of ABFE, BCGF, CDHG and DAEH:

$$\mathrm{T}=\mathrm{T_h},\quad \text{for both convections} \tag{6}$$

On the surface of ABCD:

$$\mathrm{u}=\mathrm{u_0},\quad \mathrm{T}=\mathrm{T_0}\quad (\text{forced convection}) \tag{7}$$

On the surfaces of ABCD (for natural convection) and EFGH (for both convections):

The non-reflecting conditions are held.

The Sutherland's law is adopted to evaluate the viscosity and the thermal conductivity as follows, respectively

$$\mu(T)=\mu_0\left(\frac{T}{T_0}\right)^{\frac{2}{3}}\frac{T_0+110}{T+110}$$
$$k(T)=\frac{\mu(T)\gamma R}{(\gamma-1)\mathrm{Pr}} \tag{8}$$

where $\rho_0=1.1842\ \mathrm{kg/m^3}$, $g=9.81\ \mathrm{m/s^2}$, $\mu_0=1.85\times10^{-5}\ \mathrm{N\,s/m^2}$, $T_0=298.0592\ \mathrm{K}$, $\gamma=1.4$, $R=287\ \mathrm{J/kg/K}$ and $\mathrm{Pr}=0.7$.

To simplify the analysis, the following dimensionless variables are made

$$\begin{aligned} &X=\frac{x}{d},\quad Y=\frac{y}{d},\quad Z=\frac{z}{d}\\ &U=\frac{u}{u_{0,Re=950}},\quad V=\frac{v}{u_{0,Re=950}},\quad W=\frac{w}{u_{0,Re=950}}\\ &l=3d\\ &t^*=t\frac{\mu_0}{\rho_0 d^2}\\ &T^*=\frac{T}{T_h} \end{aligned} \tag{9}$$

where $u_{0,\mathrm{Re}=950}$ means a uniform velocity u_0 to be assigned at the inlet under the situation of Re = 950.

To investigate the heat transfer in the cases of different Richardson numbers, the compressibility and viscosity of the working fluid are considered. Definitions of Reynolds number, Re, Richardson number, Ri, and Rayleigh number, Ra, are represented as follows, respectively

$$\mathrm{Re}=\frac{\rho_0 u_0 d}{\mu_0} \tag{10}$$

$$Ri=\frac{Gr}{Re^2}=\frac{g\rho_0^2\beta(T_h-T_0)d^3}{\mu_0^2}\bullet\frac{\mu_0^2}{\rho_0^2u_0^2d^2}=\frac{g\beta d(T_h-T_0)}{u_0^2} \tag{11}$$

$$Ra=\mathrm{Pr}\cdot Gr=(0.7)\cdot\frac{g\rho_0^2\beta(T_h-T_0)d^3}{\mu_0^2} \tag{12}$$

3. Numerical method

Methods of the Roe scheme [16] and preconditioning [17] are adopted to resolve the governing equations of the compressible flow shown in Eq. (1). Besides, the dual time stepping method is added to calculate transient states. And Eq. (13) can be obtained

$$\Gamma\frac{\partial U_p}{\partial\tau}+\frac{\partial U}{\partial t}+\frac{\partial F_1}{\partial x}+\frac{\partial F_2}{\partial y}+\frac{\partial F_3}{\partial z}=S \tag{13}$$

where τ is an artificial time, t is a physical time. Γ is a preconditioning matrix proposed by Weiss and Smith [17] and U_P is a primitive form of $[\rho,\rho u,\rho v,\rho w,\rho e]^T$. By the discretization of Eqs. (13) and (14) can be obtained. Terms of the $\frac{\partial U_p}{\partial\tau}$ and $\frac{\partial U}{\partial t}$ are differentiated by a first-order forward and a second-order backward differences, respectively. Terms of the $\frac{\partial F_1}{\partial x}$, $\frac{\partial F_2}{\partial y}$ and $\frac{\partial F_3}{\partial z}$ are differentiated by a central difference

$$\begin{aligned} &\Gamma\frac{U_p^{k+1}-U_p^k}{\Delta\tau}+\frac{3U^{n+1}-4U^n+U^{n-1}}{2\Delta t}+\frac{1}{\Delta x}\left(F^k_{1_{i+\frac12,j,k}}-F^k_{1_{i-\frac12,j,k}}\right)\\ &+\frac{1}{\Delta y}\left(F^k_{2_{i,j+\frac12,k}}-F^k_{2_{i,j-\frac12,k}}\right)+\frac{1}{\Delta z}\left(F^k_{3_{i,j,k+\frac12}}-F^k_{3_{i,j,k-\frac12}}\right)=S \end{aligned} \tag{14}$$

Afterward terms of the U^{k+1} and F_i^{k+1} in Eq. (14) are necessary to be linearized and expressed as follows, respectively

$$U^{k+1}=U^k+M\Delta U_p \tag{15}$$

where $M=\frac{\partial U}{\partial U_p}$ and $\Delta U_p=U_p^{k+1}-U_p^k$

$$F_1^{k+1}=F_1^k+A_p\Delta U_p \tag{16}$$

where the $A_p=\frac{\partial F_1^k}{\partial U_p}$ is the flux Jacobian and the same method is used for the $B_p=\frac{\partial F_2^k}{\partial U_p}$ and $C_p=\frac{\partial F_3^k}{\partial U_p}$ in linearization of the F_2^{k+1} and F_3^{k+1}, respectively.

To substitute Eqs. (15) and (16) into Eq. (14), the following equation is obtained

$$\begin{aligned} &\Gamma\frac{U_p^{k+1}-U_p^k}{\Delta\tau}+\frac{3U^{k+1}-4U^n+U^{n-1}}{2\Delta t}+\delta_x\left(F_1^k+A_p\Delta U_p\right)\\ &+\delta_y\left(F_2^k+B_p\Delta U_p\right)+\delta_z\left(F_3^k+C_p\Delta U_p\right)=S^k \end{aligned} \tag{17}$$

where δ_x, δ_y, and δ_z are central-difference operators.

Eq. (17) can be rearranged as the following form

$$\left[\frac{I}{\Delta\tau}+\Gamma^{-1}M\frac{3}{2\Delta t}+\Gamma^{-1}\left(\delta_xA_p^k+\delta_yB_p^k+\delta_zC_p^k\right)\right]\Delta U_p=\Gamma^{-1}R^k \tag{18}$$

where $R^k=S-\left(\frac{3U^k-4U^n+U^{n-1}}{2\Delta t}\right)-(\delta_xF_1^k+\delta_yF_2^k+\delta_zF_3^k)$

To solve a problem of the convergence of a low-speed compressible flow, the solver of.

Eq. (19) is newly derived from the LUSGS implicit method originally proposed by Yoon and Jamesont [18]

$$\begin{aligned} &A_p=\Gamma^{-1}A_p^k\\ &B_p=\Gamma^{-1}B_p^k\\ &B_p=\Gamma^{-1}C_p^k \end{aligned} \tag{19}$$

A_p, B_p and C_p can be divided into two parts

$$\begin{aligned} &A_p=A_p^+ + A_p^-\\ &B_p=B_p^+ + B_p^-\\ &C_p=C_p^+ + C_p^- \end{aligned} \tag{20}$$

where

$$\begin{aligned} &A_p^\pm=\frac12(A_p\pm|\lambda_A|I)\\ &B_p^\pm=\frac12(B_p\pm|\lambda_B|I)\\ &C_p^\pm=\frac12(C_p\pm|\lambda_C|I) \end{aligned} \tag{21}$$

To substitute Eq. (20) into Eq. (18), the following equation is obtained

$$\begin{aligned} &\left[\frac{I}{\Delta\tau}+\Gamma^{-1}M\frac{3}{2\Delta t}+\delta_\xi\left(A_p^++A_p^-\right)+\delta_\eta\left(B_p^++B_p^-\right)+\delta_\zeta\left(C_p^++C_p^-\right)\right]\Delta U_p\\ &=\Gamma^{-1}R^k \end{aligned} \tag{22}$$

$\delta_\xi\left(A_p^++A_p^-\right)$ can be derived as following equation

$$\delta_\xi\left(\tilde A_p^++\tilde A_p^-\right)=\delta_\xi^-\tilde A_p^++\delta_\xi^+\tilde A_p^-=\frac{\tilde A_{p,i}^+-\tilde A_{p,i-1}^+}{\Delta\xi}+\frac{\tilde A_{p,i+1}^--\tilde A_{p,i}^-}{\Delta\xi} \tag{23}$$

To substitute Eq. (23) into Eqs. (22) and (24) can be obtained

$$\begin{aligned} &\left[\frac{I}{\Delta\tau}+\Gamma^{-1}M\frac{3}{2\Delta t}+\frac{\widetilde A_{p,i}^+-\widetilde A_{p,i-1}^+}{\Delta\xi}+\frac{\widetilde A_{p,i+1}^--\widetilde A_{p,i}^-}{\Delta\xi}+\frac{\widetilde B_{p,j}^+-\widetilde B_{p,j-1}^+}{\Delta\eta}\right.\\ &\left.+\frac{\widetilde B_{p,j+1}^--\widetilde B_{p,j}^-}{\Delta\eta}+\frac{\widetilde C_{p,k}^+-\widetilde C_{p,k-1}^+}{\Delta\zeta}+\frac{\widetilde C_{p,k+1}^--\widetilde C_{p,k}^-}{\Delta\zeta}\right]\Delta\overline U_p=\Gamma^{-1}R^k \end{aligned} \tag{24}$$

Eq. (24) can be rearranged as follows

$$(L+D+U)\Delta U_p=\Gamma^{-1}R^k \tag{25}$$

where

Table 1
Comparisons for all situations ($Ra = 6.78 \times 10^5, \Delta T = 100K$).

Flow	$\dot{M}_{inlet}$	$\dot{M}_{outlet}$	U_0	U_{max}	$(\overline{Nu})_i$	Ri	t^*
Natural convection Re = 0	1	0	1	1.43	9.46		0.09
Mixed convection Re = 950	1	≅0	1	1.46	8.87	1.0	0.07
Mixed convection Re = 400	0.43	0.02	0.46	1.27	7.16	5.9	0.07
Mixed convection Re = 200	0.21	0.12	0.22	1.13	7.71	23.6	0.09
Mixed convection Re = 100	0.11	0.11	0.11	0.95	7.64	94.2	0.09

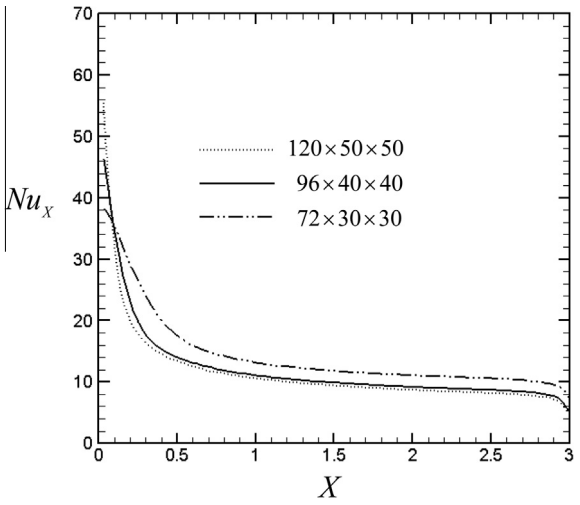

Fig. 2. Grid distributions under natural convection ($Ra = 6.78 \times 10^5, \Delta T = 100K$).

$$L = -\left[\frac{1}{\Delta\xi}(A_p^+)_{i-1,j,k} + \frac{1}{\Delta\eta}(B_p^+)_{i,j-1,k} + \frac{1}{\Delta\zeta}(C_p^+)_{i,j,k-1}\right]$$

$$D = \frac{I}{\Delta\tau} + \Gamma^{-1}M\frac{3}{2\Delta t} + \left[\frac{1}{\Delta\xi}((A_p^+)_{i,j,k} - \left(A_p^-\right)_{i,j,k}) + \frac{1}{\Delta\eta}((B_p^+)_{i,j,k} - (B_p^-)_{i,j,k}) + \frac{1}{\Delta\zeta}((C_p^+)_{i,j,k} - (C_p^-)_{i,j,k})\right]$$

$$U = \left[\frac{1}{\Delta\xi}\left(A_p^-\right)_{i+1,j,k} + \frac{1}{\Delta\eta}(B_p^-)_{i,j+1,k} + \frac{1}{\Delta\zeta}(C_p^-)_{i,j,k+1}\right]$$

As for the computation of $R^k = S - \left(\frac{3U^k - 4U^n + U^{n-1}}{2\Delta t}\right) - \left(\delta_x F_1^k + \delta_y F_2^k + \delta_z F_3^k\right)$ in the RHS (right hand side) of Eq. (18), terms of the F_i in Eq. (3) based on the Cartesian coordinate can be divided into two parts. One is an inviscid term $F_{inviscid}$

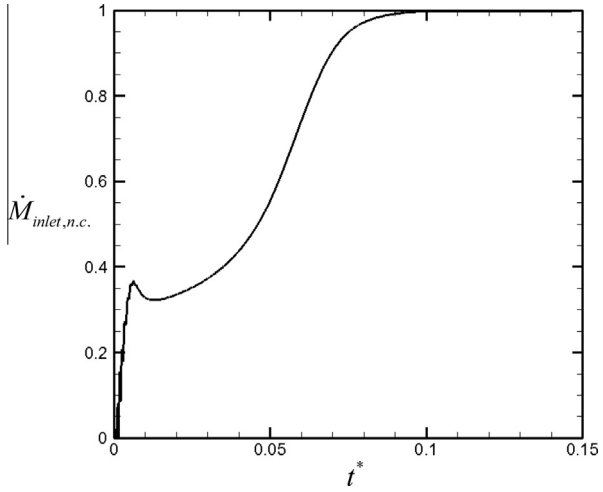

Fig. 3. Variation of mass flow rate with time for natural convection at the inlet ($Ra = 6.78 \times 10^5, \Delta T = 100K$).

$$F_{inviscid} = \begin{pmatrix} \rho u_i \\ \rho u_i u + P\delta_{i1} \\ \rho u_i v + P\delta_{i2} \\ \rho u_i w + P\delta_{i3} \\ (\rho e + P)u_i \end{pmatrix} \tag{26}$$

The other is a viscous term $F_{viscous}$

$$F_{viscous} = -\begin{pmatrix} 0 \\ \mu A_{i1} \\ \mu A_{i2} \\ \mu A_{i3} \\ \mu A_{ij}u_j + \lambda\frac{\partial T}{\partial x_i} \end{pmatrix} \tag{27}$$

A Roe upwind difference scheme [16] is employed in discretization of the terms of the $F_{inviscid}$ at the cells interface $(i+\frac{1}{2})$ and expressed as follows at a low Mach number situation

$$F_{inviscid,i+\frac{1}{2}} = \frac{1}{2}(F_R + F_L) - \frac{1}{2}\left\{|\Gamma^{-1}A_p|\Delta U_P\right\} \tag{28}$$

The MUSCL scheme with a third order proposed by Abalakin et al. [19] is used to compute the terms of the $F_{invicid}$, and the related derivative terms of $A_{ij} = \frac{\partial u_j}{\partial x_i} + \frac{\partial u_i}{\partial x_j}$ in Eq. (27) are computed by a fourth order central difference

$$\frac{\partial u}{\partial x} = \frac{u_{i-2} - 8u_{i-1} + 8u_{i+1} - u_{i+2}}{12\Delta x} + o(\Delta x^4) \tag{29}$$

The advantage of usage of the LUSGS implicit method is to improve efficiency.

On the heat surface, the boundary conditions are

$$\begin{aligned} P(i,0,k) &= P(i,1,k) \\ u(i,0,k) &= -u(i,1,k) \\ v(i,0,k) &= -v(i,1,k) \\ w(i,0,k) &= -w(i,1,k) \\ T(i,0,k) &= 2T_h - T(i,1,k) \end{aligned} \tag{30}$$

Where T_h is the wall temperature.

0 indicates the ghost cell and 1 indicates the cell most near the wall.

As for the boundary conditions at the outlet, in order to avoid the flow in the channel polluted by the reflections of acoustic waves induced by the compressible flow, the non-reflecting boundary conditions are then necessarily used at the outlet of the channel.

In a high speed compressible flow condition, the method of LODI (local one-dimensional inviscid relations) proposed by Poinsot and Lele [20] was suitably adopted for determining the non-reflecting boundary conditions at the outlet. However, a preconditioning matrix is not necessary in the above method that causes the method to be not adopted appropriately for determining the non-reflecting boundary conditions at the outlet under a low speed compressible flow. As a result, the method developed by Fu et al. [15] is necessary for resolving the non-reflection boundary conditions under a low speed compressible flow.

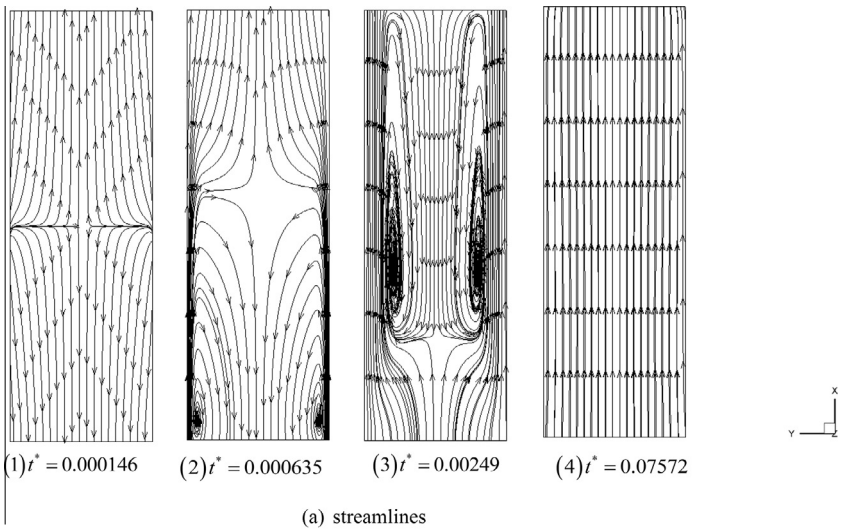

Fig. 4. Distributions of streamlines and thermal field for natural convection.

A procedure calculating the equations mentioned above is briefly described as follows.

(1) Assign the inlet conditions of pressure, velocity and temperature.
(2) Use the MUSCL method to calculate Eq. (18) to obtain the magnitude of the ΔU_P.
(3) Substitute the magnitude of the ΔU_P into Eq. (28) and use the Roe method to calculate the magnitudes of inviscid terms of the $F_{inviscid}$.
(4) Calculate Eq. (29) to obtain the magnitudes of viscous terms and substitute in Eq. (27).
(5) Solve U_p^{k+1}

$$U_p^{k+1} = U_p^k + \Delta U_p^k \tag{31}$$

(6) Calculate Eq. (14) and examine the convergence of the iterational computation of U_p^{k+1}. Repeat (2) ~ (5) until until $\frac{U_p^{k+1} - U_p^k}{\Delta\tau} < \varepsilon$, $\varepsilon = 10^{-3}$.

4. Results and discussion

In this study, there are five situations of which the ratio of the height to the width is 3, tabulated in Table 1 to be performed. Rayleigh number is 6.78×10^5 in those five situations. The mass flow rate of the situation of Re = 950 assigned in mixed convection is the same as that obtained by the situation of natural convection. The definition of the dimensionless mass flow rate at the inlet $\dot{M}_{inlet}$ and the dimensionless mass flow rate sucked from the outside $\dot{M}_{outlet}$ are presented as follows, respectively

$$\dot{m}_{\mathrm{Re}=950} = \rho d^2 u_{0,\mathrm{Re}=950} \tag{32}$$

$$\dot{M}_{inlet} = \rho u_0 d^2 / \dot{m}_{\mathrm{Re}=950} \tag{33}$$

$$\dot{M}_{outlet} = \rho |u_{outlet}| d^2 / \dot{m}_{\mathrm{Re}=950}, u_{outlet} < 0 \tag{34}$$

The total mass flow rate which flows out of the channel and has advantage to heat transfer rates of heat walls is obtained by the addition of $\dot{M}_{inlet}$ and $\dot{M}_{outlet}$. In situations of mixed convection of Re = 400, 200 and 100, the mass flow rates of $\dot{M}_{outlet}$ are mainly caused by the amount of fluid to be sucked from the outside. The reason is suggested as that the strength of the driving force of natural convection is larger than those of forced convections assigned in mixed convections under situations of large magnitudes of the Richardson numbers. However, the viscous dissipation and impingement between the $\dot{M}_{inlet}$ and $\dot{M}_{outlet}$ occurring in situations of Re = 400, 200 and 100 cannot avoid. The total mass flow rates of situations of Re = 400, 200 and 100 have difficulty to be equal to that of the situation of natural convection. The dimensionless time t^* are from $t^* = 0$ to the steady state for situations of Re = 0,

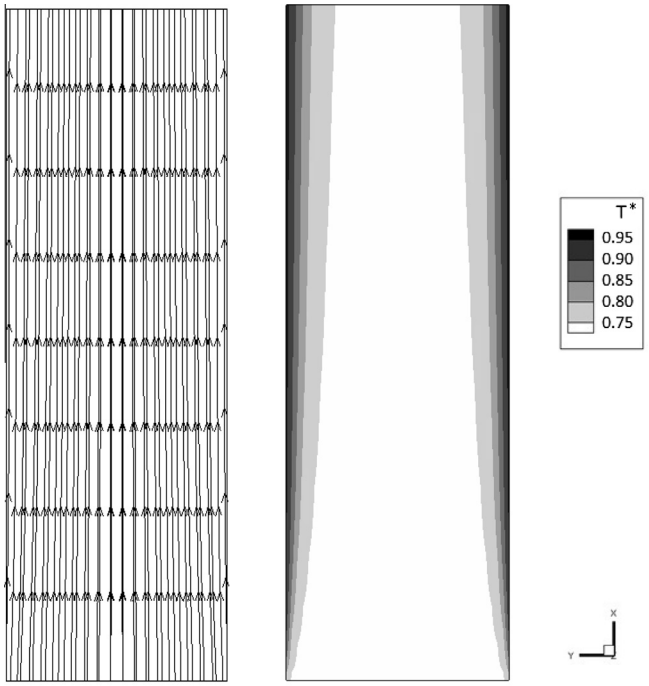

Fig. 5. Distributions of streamlines and thermal field for the Reynolds number of 950.

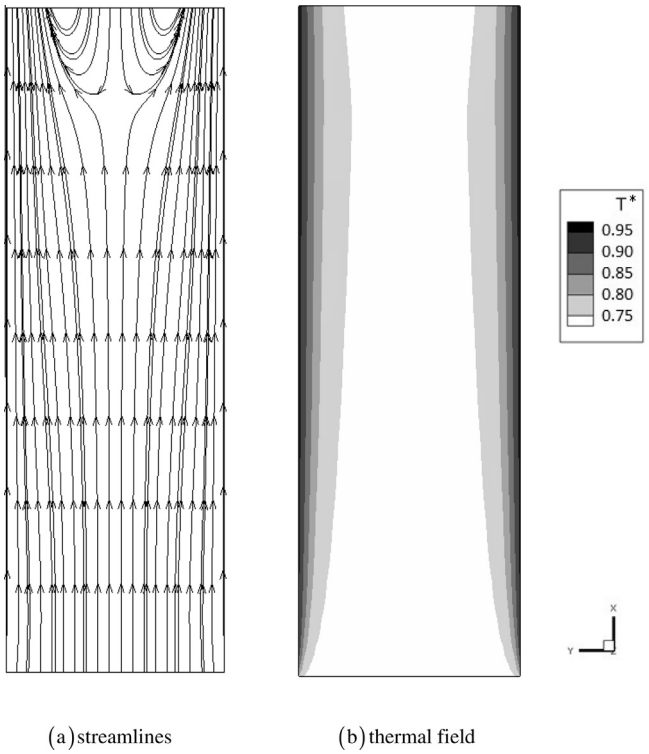

Fig. 6. Distributions of streamlines and thermal field for the Reynolds number of 400.

950, 400, and the beginning of fully unsteady state for situations of Re = 100 and 200, respectively.

Shown in Fig. 2, the results of local Nusselt numbers with different grid distributions along x axis are indicated, and the grid distributions of $120 \times 50 \times 50$, $96 \times 40 \times 40$ and $72 \times 30 \times 30$ in x, y, z directions under natural convection are tested. According to the results of local Nusselt numbers, the grid distribution of $96 \times 40 \times 40$ is adopted. The definition of the local Nusselt number Nu_x is expressed as follows

$$Nu_x = \frac{d}{k_0(T_h - T_0)}\left[k(T)\frac{\partial T}{\partial z}\right] \tag{35}$$

Shown in Fig. 3, the variation of the mass flow rate with time for natural convection at the inlet is indicated. The mass flow rate sharply increases at an initial stage, and reaches a plateau of development gradually. The negative magnitude at the initial stage indicates part of the amount of fluid originally staying in the channel to be expanded by the heat wall and extruded to the outside. The definition of the dimensionless mass flow rate $\dot{M}_{inlet,n.c.}$ is presented as follows

$$\dot{M}_{inlet,n.c.} = \rho u_{inlet} d^2 / \dot{m}_{Re=950} \tag{36}$$

Shown in Fig. 4, the variations of the streamlines and thermal field with time for natural convection are indicated. At first the high temperature of the heat surface causes the densities of the fluids in the channel to become small, and then the volume of the fluid is expanded that causes the fluids to flow out of the channel shown in Fig. 4(a1). Accordingly, the fluids near the inlet region gradually form flow reversal shown in Fig. 4(a2–3) in order to supplement the lack of the fluids which are discharged mentioned above. Accompanying with the increment of time, because of the influence of natural convection the flow field becomes steady and all the fluids flow into the channel from the inlet shown in Fig. 4a(d). In addition, orderly thermal boundary layers are observed as the flow field reaches the steady state show in Fig. 4(b).

Shown in Fig. 5, the distributions of the streamlines and thermal field for the Reynolds number of 950 are indicated, respectively. The darker the color is, the higher the temperature is shown. Because of the same mass flow rate at the inlet of both situations of natural convection and Re = 950, the streamlines and thermal filed for the Reynolds number of 950 are similar to the situation of natural convection shown in Fig. 4(a4) and Fig. 4(b), respectively.

Shown in Fig. 6, the distributions of streamlines and thermal field for the Reynolds number of 400 are indicated, respectively. In Fig. 6(a), a part of the fluids via the outlet are sucked into the channel from the outside, and a region of the flow reversal is observed. The Rayleigh number of this situation is the same with that of natural convection shown in Fig. 4, based upon the reason mentioned above and then the mass flow rate at the inlet of the situation of Re = 400 is smaller than that of natural convection. As a result, via the outlet the insufficiency of the mass flow rate is supplemented by the fluids from the outside. As well, in Fig. 6(b) the flow reversal depresses the thermal field near the outlet that somewhat increases the heat transfer rate of the region near the outlet.

In Fig. 7, the variations of streamlines with time for the Reynolds number of 200 are indicated. From Table 1, at the inlet the mass flow rate of natural convection is much larger than that of the situation of Re = 200 that causes the insufficient mass flow rate to be supplemented from the outside of the channel. Then some fluids via the central region of the outlet flows into the channel and impinges the amount of fluid provided by forced convection flowing upwards from the inlet. Afterward, both the amounts of fluid newly coalesce and form a new stream flowing upward along the heat wall. Due to the occurrence of impingement, an unsteady phenomenon is apparently observed in Fig. 7(d). Naturally, the phenomenon is advantageous to heat transfer mechanisms of the heat wall.

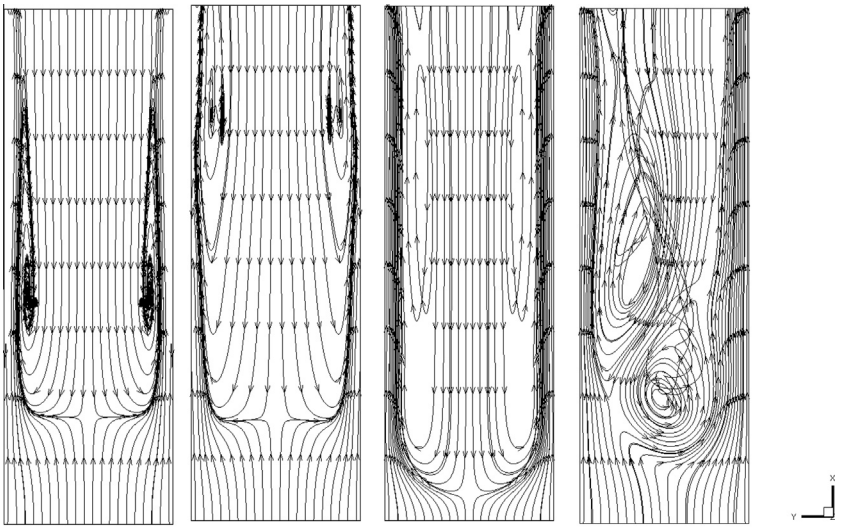

Fig. 7. Variations of streamlines with time for the Reynolds number of 200.

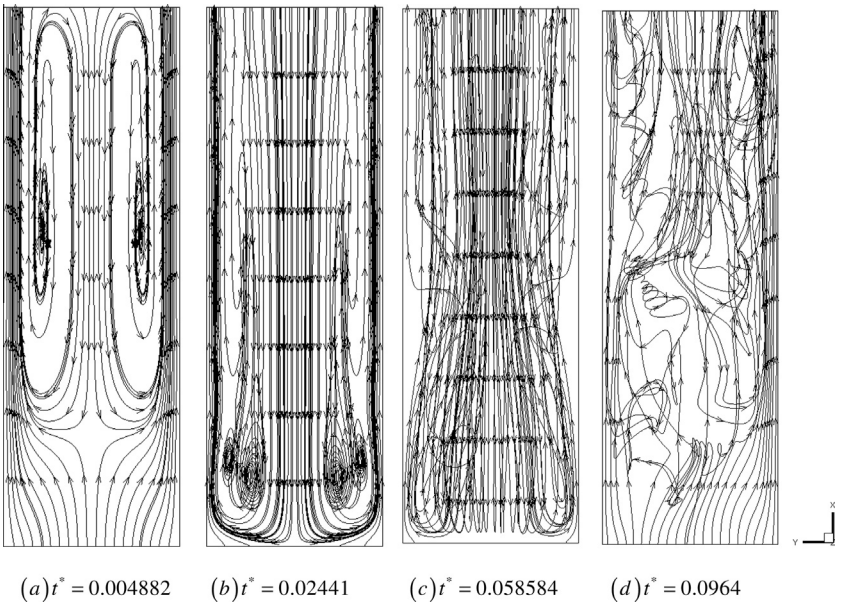

Fig. 8. Variations of streamlines with time for the Reynolds number of 100.

The variations of streamlines with time for the Reynolds number of Re = 100 are shown in Fig. 8. Since the mass flow rate at the inlet of this situation is also much less than that of the situation of natural convection. The location of the impingement caused by $\dot{M}_{inlet}$ and $\dot{M}_{outlet}$ is more close to the inlet than that shown in Fig. 7. This phenomenon leads more drastic impingement to occur that slightly decreases the mass flow rate of $\dot{M}_{outlet}$. Then the mass flow rate of $\dot{M}_{outlet}$ of Re = 100 is slightly smaller than that of Re = 200.

In Fig. 9, the variations of thermal field with time corresponding to streamlines shown in Fig. 8 are indicated, respectively. In an earlier stage, a mixing effect of both the amounts of fluid mentioned above just begins, and then orderly thermal boundary layers are observed on heat walls. Gradually, the mixing effect becomes complex and drastic, and then orderly thermal boundary layers are no longer observed on heat walls and high temperature fluids are irregularly distributed in the channel.

Time averaged local Nusselt numbers distributed on the central line of the heat surface of all situations are indicated in Fig. 10, respectively. The definition of the time averaged local Nusselt number $(Nu_x)_t$ is expressed as follows. The time interval t is calculated from $t^* = 0$ to 0.15

$$(Nu_x)_t = \frac{1}{t}\int \frac{d}{k_0(T_h - T_0)}\left[k(T)\frac{\partial T}{\partial z}\right]dt \tag{37}$$

In the front region ($x < 0.5$), under the situation of natural convection the amount of fluid begins to be sucked from the outside of the channel and flows into the channel. The buoyancy force driving the amount of fluid to flow upwards is gradually strengthened, and then the upward velocity is also accelerated little by little. Oppositely, under the situation of forced convection a certain quantity of mass flow rate is evenly provided at the inlet to flow into the channel. As a result, in this region time averaged local Nusselt

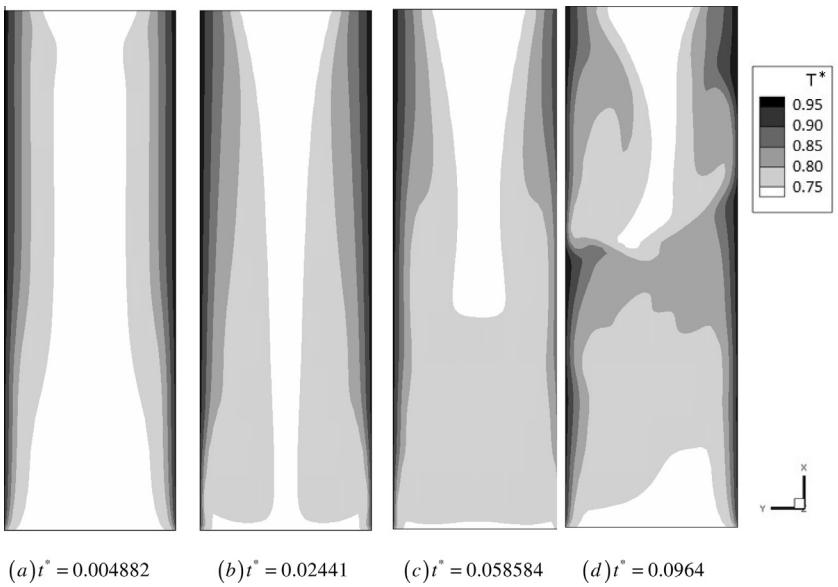

Fig. 9. Variations of thermal field with time for the Reynolds number of 100.

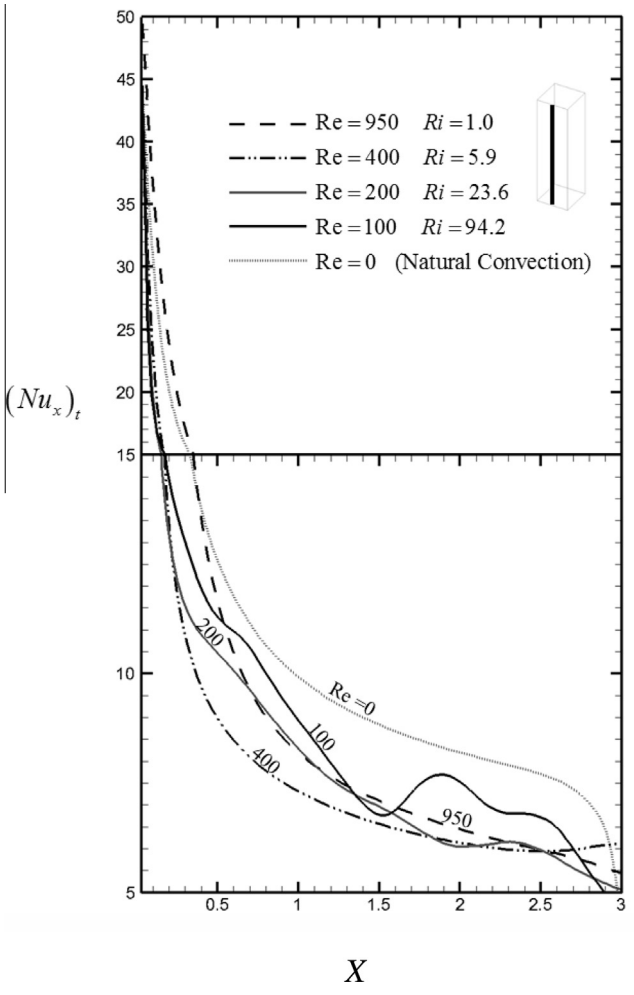

Fig. 10. Time averaged local Nusselt numbers on the central line of the heat surface.

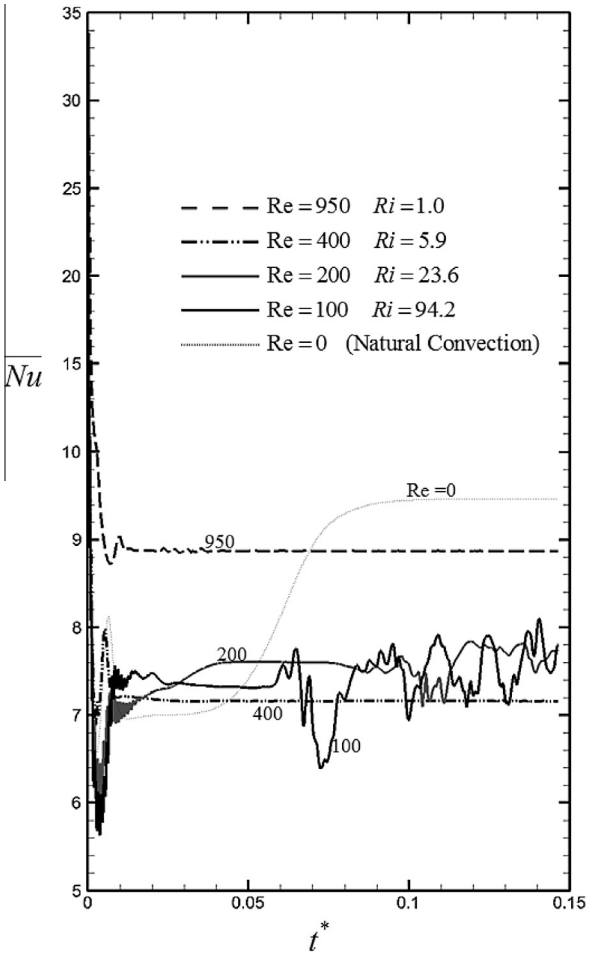

Fig. 11. Variations of area averaged Nusselt numbers with time.

numbers of the situation of Re = 950 are slightly larger than those of the situation of natural convection. The other situations of forced convection, mass flow rates at the inlet are smaller than the mass flow rate of the situation of natural convection at the inlet. Naturally, time averaged local Nusselt numbers of the other three

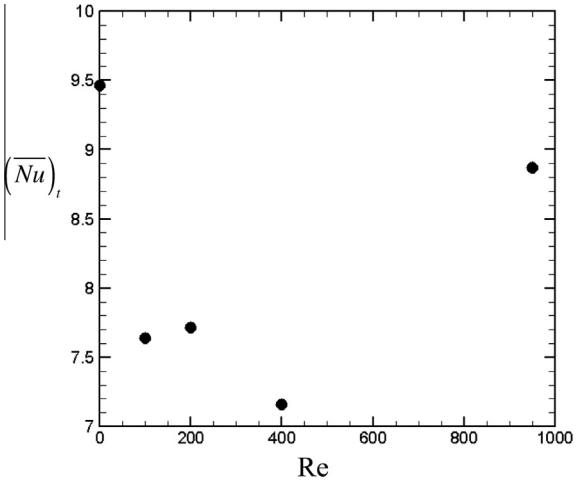

Fig. 12. Variations of time and area averaged Nusselt numbers with different Reynolds numbers.

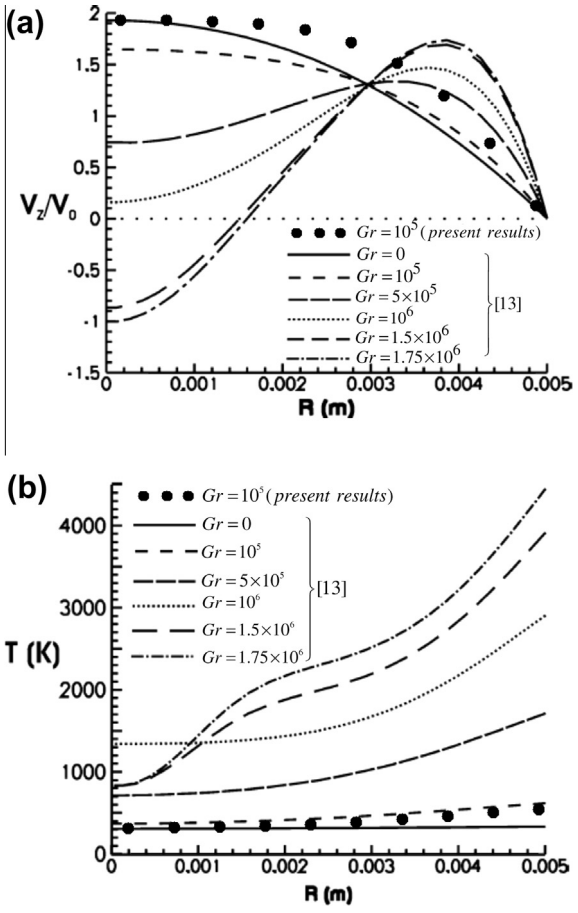

Fig. 13. Comparisons of distributions of velocities and temperature of present results with those of the previous work [13].

situations of forced convection are smaller than that of the situation of natural convection. Beyond the front region, under the situation of natural convection the upward fluid driven by the buoyancy force which is gradually strengthened is mainly concentrated on the heat surface. Then time averaged local Nusselt numbers of natural convection are larger than those of situations of forced convection in

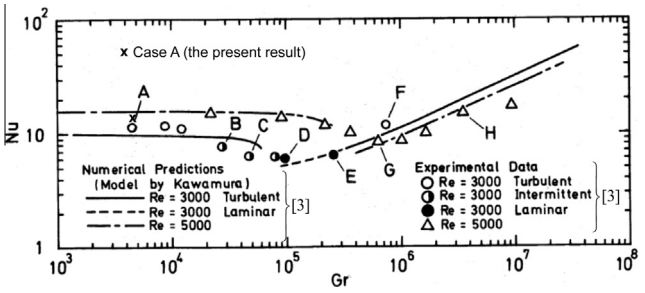

Fig. 14. Comparison of the average Nusselt number of the present result with that of the previous work [3].

which the mass flow rate is evenly distributed on the cross section. According to the statements mentioned above, in situations of lower Reynolds numbers (Re = 100 and 200) via the outlet the fluids are sucked into the channel and impinges the upward fluid provided by forced convection. This phenomenon causes the drastic impingement to occur in the channel. Consequently, time averaged local Nusselt numbers of the situations of lower Reynolds numbers (Re = 100 and 200) are larger than those of the situation of Re = 400. Near the outlet region, a part of time averaged local Nusselt numbers of the situation of Re = 100 are even larger than those of the situation of Re = 950. However, the mass flow rate of the situation of Re = 400 is medium and slightly smaller than that of the situation of natural convection. The amount of fluid sucked into the channel from the outside is small and has no ability to disturb the flow field provided by forced convection. The smallest distribution of time averaged local Nusslet numbers is then indicated.

Fig. 11 indicates the variations of area averaged Nusselt numbers with time. The definition of area averaged Nusselt number $\overline{Nu}$ is defined as follows

$$\overline{Nu} = \frac{1}{A}\int\int_A Nudxdy = \frac{1}{A}\int\int_A \frac{d}{k_0(T_h - T_0)}\left[k(T)\frac{\partial T}{\partial z}\right]dxdy \qquad (38)$$

In an earlier time region, natural convection begins to develop that causes the magnitudes of area averaged Nusselt numbers of natural convection to be smaller than those of situations of forced convection. After a certain developing time, according to the reasons mentioned above the magnitudes of the area averaged Nusselt numbers of natural convection are gradually larger than those of situations of forced convection. Among situations of forced convection, the magnitudes of the area averaged Nussslt numbers of the situation of Re = 950 situation are apparently larger than those of the other three situations of forced convection. According to the reason suggested above, the magnitudes of area averaged Nusselt numbers of the situation of Re = 400 are smaller than those of the other two situations of Re = 100 and 200. The similar phenomena of the flow reversal are found out in situations of Re = 100 and 200. The deviation of the magnitudes of situations of Re = 100 and 200 is small.

In Fig. 12, the variation of time and area averaged Nusselt numbers of all situations is indicated. The definition of the time and area averaged Nusselt number is expressed as follows

$$(\overline{Nu})_t = \frac{1}{t}\int_t \overline{Nu}dt \qquad (39)$$

According to the reasons mentioned above, the maximum and minimum magnitudes of the time and area averaged Nusselt numbers are situations of natural convection and Re = 400, respectively. The difference of the magnitudes of situations of Re = 100 and 200 is slight. The magnitude of the time and area averaged Nusselt number of natural convection is slightly larger than that of the situation of Re = 950. The main reason is suggested as that the amount of

fluid provided by forced convection is evenly distributed in the cross section of the channel, and the amount of fluid in the channel induced by natural convection is mainly concentrated on heat walls.

In Fig. 13, comparisons of distributions of temperature and velocity of present results with those of the previous work [13] are indicated, respectively. The physical model of the previous work was a circular cylinder, then an equivalent hydraulic diameter regarded as the width of a square duct is used to calculate distributions of temperature and velocity on the center line of the outlet cross section. The trend of both results is consistent. Since geometries of the two models are different, the existences of the slight deviations between both results are reasonable.

In Fig. 14, comparison of the present result with that of an experimental result of [3] is shown. For the Reynolds number and heat flux of both situations are 3000 and 57 $W \cdot m^{-2}$, respectively. The ratio of the height to the width is 10 in this work because of the limitation of computation memory, and the ratio of [3] was 25. The shorter the height is, the larger the average Nusselt number is achieved. Naturally, the result of this work ought to be larger than that of [3].

5. Conclusions

An investigation of flow reversal of mixed convection in a three dimensional rectangular channel with the consideration of the compressibility of the working fluid is studied numerically. The occurrence of flow reversal of mixed convection in the channel is mainly depended by the balance of mass flow rates induced by natural convection and provided by forced convection. The mass flow rate induced by natural convection is larger than that provided by forced convection at the inlet that causes the phenomenon of flow reversal to occur easily. The phenomenon will decay accompanying with the decrement of the difference between both mass flow rates. In the range of this work, several related features of the results are drawn as follows.

1. The magnitude of Richardson number dominates the mechanisms of the flow reversal of mixed convection.
2. Drastic phenomena of the flow reversal of mixed convection are mainly caused by the mutual impingement between the amount of downward fluid sucked from the outlet and the amount of upward fluid from the inlet provided by forced convection.
3. Under the same mass flow rate, the magnitude of time and area averaged Nusselt number of natural convection is slightly superior to that of mixed convection

Acknowledgement

The authors gratefully acknowledge the support of the Natural Science Council, Taiwan, ROC under Contact NSC100-2221-E-009-086-MY2

References

[1] B. Metais, E.R.G. Eckert, Forced, mixed, and free convection regimes, J. Heat Transfer 86 (1964) 295–296.
[2] A. Behzadmehr, N. Galanis, A. Laneville, Low Reynolds number mixed convection in vertical tubes with uniform wall heat flux, Int. J. Heat Mass Transfer 46 (2003) 4823–4833.
[3] H. Tanaka, S. Maruyama, S. Hatano, Combined forced and natural convection heat transfer for upward flow in a uniformly heated, vertical pipe, Int. J. Heat Mass Transfer 30 (1987) 165–174.
[4] G.P. Celataa, F. D'Annibalea, A. Chiaradia, M. Cumo, Upflow turbulent mixed convection heat transfer in vertical pipes, Int. J. Heat Mass Transfer 41 (1998) 4037–4054.
[5] K. Boulama, N. Galanis, Analytical solution for fully developed mixed convection between parallel vertical plates with heat and mass transfer, J. Heat Transfer 126 (2004) 381–388.
[6] G. Desrayaud, G. Lauriat, Flow reversal of laminar mixed convection in the entry region of symmetrically heated, vertical plate channels, Int. J. Therm. Sci. 48 (2009) 2036–2045.
[7] M. Zghal, N. Galanis, C.T. Nguyen, Developing mixed convection with aiding buoyancy in vertical tubes: a numerical investigation of different flow regimes, Int. J. Therm. Sci. 40 (2001) 816–824.
[8] D.B. Ingham, D.J. Keen, P.I. Heggs, Two dimensional combined convection in vertical parallel plate ducts, including situations of flow reversal, Int. J. for Numer. Methods Eng. 26 (1973) 1645–1664.
[9] A. Barletta, Analysis of flow reversal for laminar mixed convection in a vertical rectangular duct with one or more isothermal walls, Int. J. Heat Mass Transfer 44 (2001) 3481–3497.
[10] A. Barletta, Fully developed mixed convection and flow reversal in a vertical rectangular duct with uniform wall heat flux, Int. J. Heat Mass Transfer 45 (2002) 641–654.
[11] A. Barletta, Laminar convection in a vertical channel with viscous dissipation and buoyancy effects, Int. J. Heat Mass Transfer 41 (1998) 3501–3513.
[12] C.S. Yang, D.Z. Jeng, K.A. Yih, C. Gau, W. Aung, Numerical and analytical study of reversed flow and heat transfer in a heated vertical duct, J. Heat Transfer 131 (2009).
[13] C.T. Nguyen, S.B. Maïga, M. Landry, N. Galanis, G. Roy, Numerical investigation of flow reversal and instability in mixed laminar vertical tube flow, Int. J. Therm. Sci. 43 (2004) 797–808.
[14] D.D. Gray, A. Giorigini, The validity of Boussinesq approximation for liquids and gases, Int. J. Heat Mass Transfer 19 (1976) 545–551.
[15] W.S. Fu, C.G. Li, C.C. Tseng, An investigation of a dual-reflection phenomenon of a natural convection in a three dimensional horizontal channel without Boussinesq assumption, Int. J. Heat Mass Transfer 53 (2010) 1575–1585.
[16] P.L. Roe, Approximation Riemann solver, parameter vectors, and difference schemes, J. Comput. Phys. 43 (1981) 357–372.
[17] J.M. Weiss, W.A. Simth, Preconditioning applied to variable and constants density flows, AIAA 33 (1995) 2050–2056.
[18] S. Yoon, A. Jamesont, Lower–upper symmetric-Gauss–Seidel method for the Euler and Navier–Stokes equations, AIAA 26 (1988) 1025–1026.
[19] I. Abalakin, A. Dervieux, T. Kozubskaya, A vertex centered high order MUSCL scheme applying to linearised Euler acoustics, INRIA 4459 (2002).
[20] T.J. Poinsot, S.K. Lele, Boundary conditions for Navier–Stokes, J. Comput. Phys. 101 (1992) 104–129.